

Beam dynamics simulations of optically-enhanced field emission from structured cathodes

A. Seymour^{*}, D. Grote[†], D. Mihalcea^{*}, P. Piot^{*,**} and J.-L. Vay[‡]

^{*}*Northern Illinois Center for Accelerator & Detector Development and Department of Physics,
Northern Illinois University, DeKalb IL 60115, USA*

[†]*Lawrence Livermore National Laboratory, Livermore, CA 94551, USA*

^{**}*Accelerator Physics Center, Fermi National Accelerator Laboratory, Batavia, IL 60510, USA*

[‡]*Lawrence Berkeley National Laboratory, Berkeley, CA 94720, USA*

Abstract. Structured cathodes – cathodes with a segmented emission surface – are finding an increasing number of applications and can be combined with a variety of emission mechanisms, including photoemission and field emission. These cathodes have been used to enhance the quantum efficiency of metallic cathodes when operated as plasmonic cathodes, have produced high-current electron bunches through field emission from multiple tips, and can be used to form beams with transverse segmentations necessary for improving the performance of accelerator-based light sources. In this report we present recent progress towards the development of finite-difference time-domain particle-in-cell simulations using the emission process in structured cathodes based on the WARP framework. The simulations give further insight on the localized source of the emitted electrons which could be used for additional high-fidelity start-to-end simulations of electron accelerators that employ this type of electron source.

Keywords: electron sources, photoemission, field emission, beam dynamics

PACS: 29.27.-a, 41.85.-p, 41.75.F

INTRODUCTION

Electron emission from structured cathodes is finding an increasing number of applications. It was recently experimentally demonstrated that optically enhanced field emission from plasmonic cathodes could substantially enhance the electron yield [1]. Likewise structured cathodes can produce transversely segmented beams that could be used for coherent radiation generation processes [2]. One of the challenges is to fully understand the electron beam distribution: the field pattern on the cathode is locally enhanced leading to local charge variation during the emission process.

Field emission occurs from electron tunneling in the presence of a large electric field. The Fowler-Nordheim (FN) law gives the current distribution associated with an electron beam emitted in the presence of an applied macroscopic field [3]:

$$\mathbf{J}(\mathbf{x}, t) = AE(\mathbf{x}, t)^2 \exp\left(-\frac{B}{E(\mathbf{x}, t)}\right) \hat{\mathbf{n}}(\mathbf{x}), \quad (1)$$

where A and B are parameters dependent on the field emitter material and surface properties, $\hat{\mathbf{n}}(\mathbf{x})$ is a normal vector describing the local surface at the position \mathbf{x} on the emitting surface. For a flat surface, $\hat{\mathbf{n}} = \hat{\mathbf{z}}$ is aligned with the surface normal to the beam propagation. One of the challenges of field emission is to produce bunched beams. One solution would be to place a field emitter in a time-varying field (e.g., an RF field). Unfortunately placing a field emitter on the backplane of a conventional RF gun (with exposure to an electric field generated in the gun) leads to the formation of electron bunches of substantial length (typically $\sim 1/3$ of the RF gun operating wavelength). Such long bunches generally lead to poor beam quality as a substantial energy spread is acquired during acceleration within the RF gun. In addition, it can lead to significant multipacting effects [4].

A possible alternative to pulse (or gate) the field emission mechanism is to use a short laser pulse with a duration much shorter than the RF period of the field sustained in the RF gun cavity. The laser can be used to trigger photoemission [5] or enable optically-induced field emission if the fields are strong enough [6]. In this report we explore the latter case for two example configurations: one, a "gated" diamond field emitter tip; and, two, a Gaussian-profile nanohole. In this paper we present simulations of field emission for a simple DC bias cathode maintained below threshold.

To precisely understand the dynamics of the electrons in the laser-pulse fields, we rely on numerical simulations based on the finite-difference time-domain (FDTD) technique combined with the particle-in-cell (PIC) approach. We implement the model within the WARP open-source framework available from Lawrence Berkeley National Laboratory [7]. WARP is capable of solving, from first principles, arbitrary electrodynamic problems [8].

In order to include particles emitted through field emission in WARP, we implemented the Fowler-Nordheim (FN) relation (Eq. 1). The user specifies the geometry and the work function of the field emitting conductor and the current density is produced based on the time-dependent electric field evaluated just outside the conductor. The grid cells adjacent to the conductor surface are uniformly filled with charged particles at rest. The volume density of the particles is such that the FN formula is satisfied – e.g., the charge emitted during a given time step δt is $\delta Q(\mathbf{x}) = \int_S |\mathbf{J}(\mathbf{x}, t)| d^2\mathbf{x} \delta t$, where S is the area of the emitting surface. The accuracy of the model depends on the accuracy of the electric field evaluation. Therefore the size of the grid cell in the vicinity of the conductor should be small enough to finely resolve the small geometric features associated with the field emitter.

DIAMOND FIELD EMITTER

As a first example we consider a diamond field emitted array (DFEA) cathode composed of diamond tips positioned on pyramids with their extremities separated by $\sim 10 \mu\text{m}$. The cathode has a similar geometry to the one experimentally investigated in Ref. [9] and also includes an anode (see Fig. 1, left column). The anode is held at a specified potential to maintain a static electric field close to (but below) the field emission threshold in order to prevent substantial emission from occurring. A laser impinges the cathode tip and produces the necessary enhancement to enable electron emission. The emission occurs for a time comparable to the duration of the laser pulse. For this study we use the parametrization of the FN law $\mathbf{J} = \frac{k_1 E^2}{\phi} \exp\left(-\frac{k_2 \phi^3}{E}\right) \hat{\mathbf{n}}$, where the work function of the material is $\phi = 4.15 \text{ eV}$, and $k_1 = 1.54 \times 10^{-6} (\text{A eV})/\text{V}^2$ and $k_2 = 6.83 \times 10^7 \text{ V}/(\text{cm eV}^{3/2})$ are constants determined in Ref. [10].

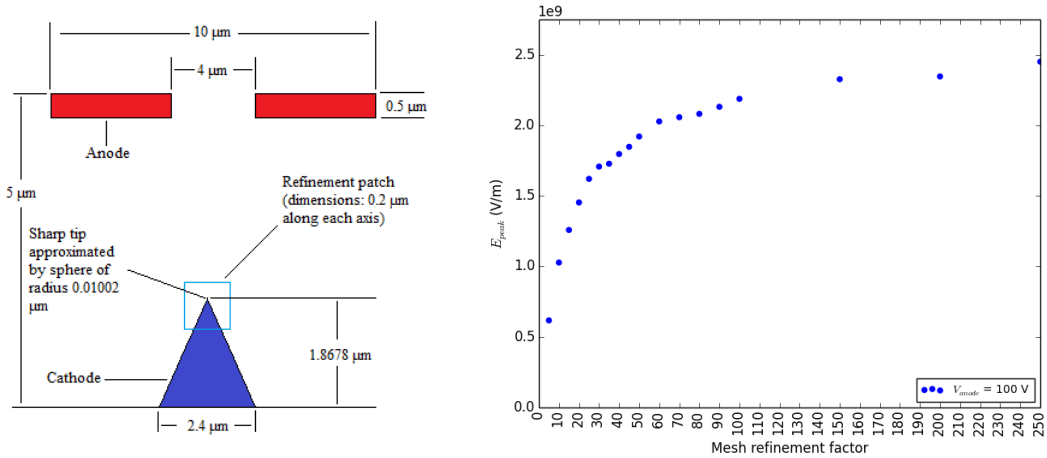


FIGURE 1. LEFT: Layout of the diamond field emission cathode (not to scale). RIGHT: Electrostatic field at the cathode tip surface as a function of mesh refinement factors for an anode voltage of 100 V with the cathode grounded.

The geometry of the cathode and anode is given in (x, z) coordinates such that they will define a surface of revolution around the x axis to generate a volume. The tip, which serves as the particle source, is approximated as a sphere and the voltage of the cathode is set to zero. Both the anode and the cathode are implemented in WARP as conductors and are also set as particle scrapers. The cathode is set as the electron source using the FN relation for particle emission. However, the current particle injection algorithm does not currently include mesh refinement.

This simulation requires two solvers – the MRBLOCK3D electrostatic (ES) solver and the EM3D electromagnetic (EM) solver – to work concurrently. In effect, the electrostatic fields are only calculated once at the beginning of the simulation and are then applied as an external field during each time step as the time-dependent simulation (involving

the laser propagation) is performed.

The evaluation of the electric field on the cathode surface is crucial as it will strongly affect the current density. Additionally, because of the "lighting-rod" effect, the electric field E at the cathode is enhanced comparably to the "macroscopic" applied electric field as $E = \beta_e E_{mac}$, where β_e is the enhancement factor. In the present case, $E_{mac} \simeq V_{anode}/d$, where d is the distance between the anode and the grounded base of the cathode. In order to appropriately choose the mesh size, we use the mesh-refinement capabilities of WARP. WARP allows the user to refine the grid of a subarea of the computational domain by dividing the nominal grid cells by a refinement factor. We explore the affect of this mesh refinement factor on the computed electric field at the tip of the field emitter (see Fig. 1). The latter figure confirms that the electric field value asymptotically converges for sufficiently large mesh refinement factors. The choice of the mesh refinement factor is essentially a compromise between accuracy and the execution time – larger refinement factors result in significantly longer computation time. We therefore select a mesh refinement factor of 50 and set the voltage of the anode to $V = 400$ V.

The electrostatic field is computed during first iteration and is then passed as external field while the time-dependent electromagnetic-field simulation is performed. The electromagnetic simulation includes the laser pulse generation and propagation in conjunction with the laser-triggered particle emission. Particle tracking is handled via the WARP particle-in-cell algorithm. For this simulation, we define the parameters as follows: the wavelength is $\lambda = 800$ nm; the normalized potential vector is $a_0 = 10 \times 10^{-3}$; the radius of the laser at the waist is taken to be $0.5 \mu\text{m}$; and the pulse duration is 1.0 fs. We take the laser to be polarized along the \hat{x} -axis. The laser is injected in the simulation four Rayleigh lengths away from the cathode tip, where it then propagates along the \hat{z} direction and focuses incident on the tip. The time step for the simulations is automatically set by WARP to satisfy the Courant condition.

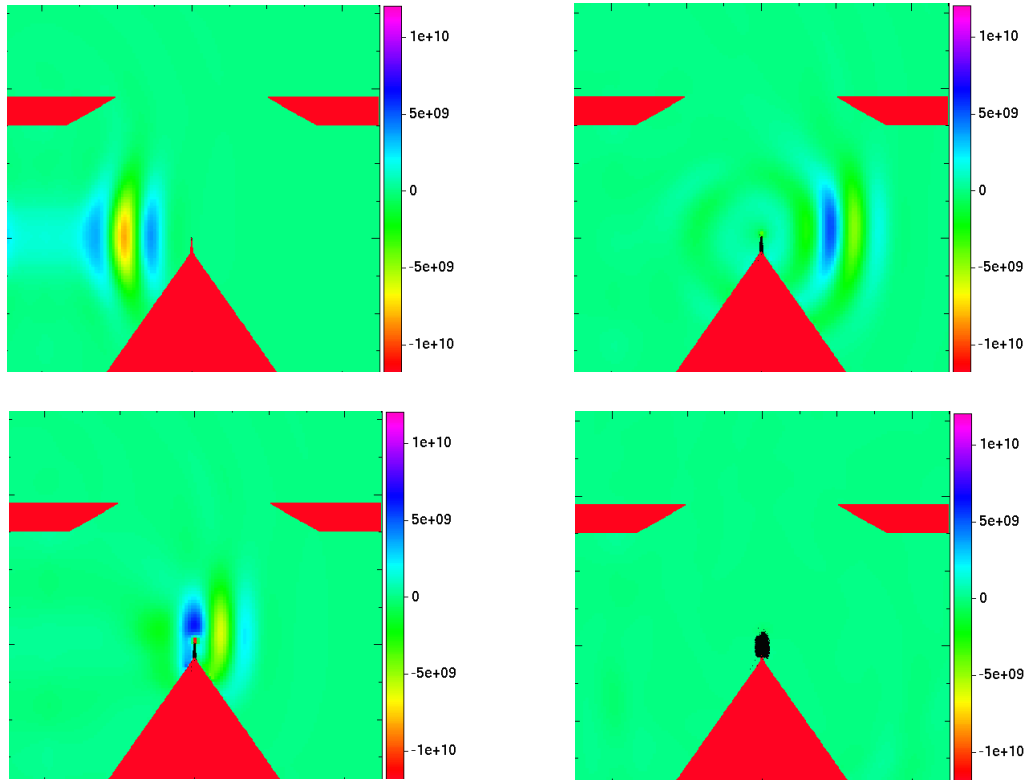


FIGURE 2. Snapshot sequence of the laser field and macro particle distribution for iteration numbers 110 (upper left), 162 (upper right), 200 (lower left), and 450 (lower right). The snapshots are taken in the $(z, y = 0, x)$ plane. The false-color contours are the electric field E_x associated with the laser pulse (in units of V/m) and the black symbols first appearing during iteration number 162 are macro particles. The laser propagates along the \hat{z} axis (i.e. from left to right). The extremity of the cathode has coordinate $(z, x) = 0$.

Snapshots of the evolution of the laser pulse and particle emission appear in Fig. 2 taken at different times to illustrate the stages in which the simulation occurs. To begin, the laser pulse originates from the left and converges (focuses) on the cathode tip located at $(x, z) = (0, 0)$. There is a shadowing effect as the laser pulse traverses the tip – that is, the left side of the tip experiences the fields from the laser before the right side does. At this point, the fields are sufficiently strong to emit electrons (macro particles) from the tip. After the laser has impinged on the tip, the laser diverges and exits the computational domain through an open boundary.

The electrons initially emitted from the cathode have such low kinetic energy that space-charge effects dominate and the electrons are repelled by their self-fields. The transverse trace space $(z, z' \equiv p_z/p_x)$ obtained at the final iteration of the simulation along with the evolution of the beam rms emittance appear in Figure 3. The trace space displays the characteristic "bow tie" pattern typically obtained in RF guns. This type of trace space leads to correlated transverse emittance dilutions that can be partially corrected using the emittance-compensation process commonly implemented in RF guns [11, 12]. In addition, some nonlinear "S-shape" distortions appear and are the consequence of spherical aberrations introduced by the "gated" anode [13]. Nevertheless, a transverse emittance below 1 nm is achieved at the anode location once the beam has attained a final kinetic energy of ~ 900 eV.

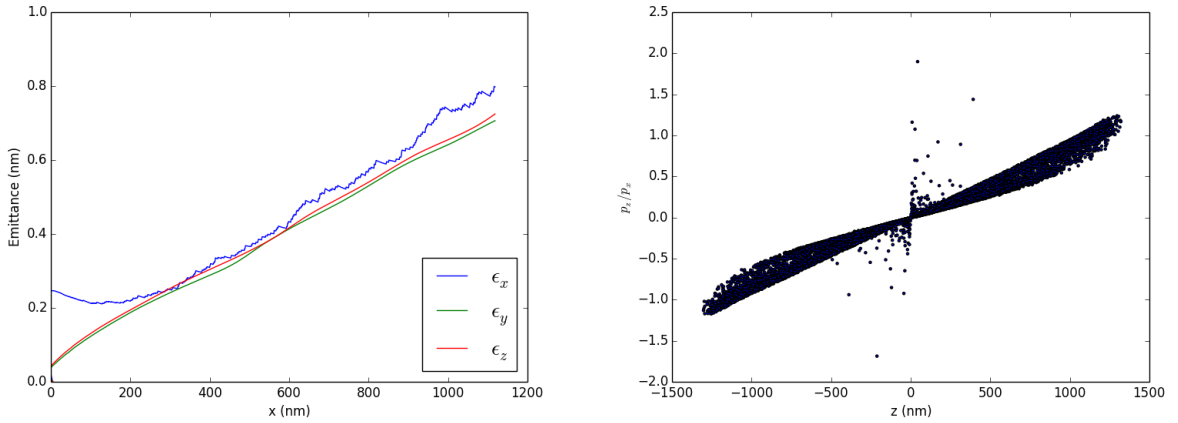


FIGURE 3. LEFT: Emittance evolution of the emitted electron bunch (the bunch propagates along the \hat{x} direction and $x = 0$ corresponds to the location of the cathode tip extremity). RIGHT: A snapshot of the transverse horizontal $(z, z' \equiv p_z/p_x)$ trace space at the final iteration corresponding to an average axial position of the bunch at $x \sim 1.0 \mu\text{m}$.

It should be noted that the emittance increase and divergence leads to significant beam loss as the macro particles with large radii are scraped by the anode [14]. The model developed is being used to optimize the cathode-anode configuration. It will also be used to investigate alternative configurations such as the head-on illumination of the tip using a longitudinally polarized laser pulse.

NANOHOLE CATHODES

We have also recently used WARP to explore the performance of plasmonic cathodes [1]. A first step is to insure the resonance effects observed in plasmonic cathodes can likewise be observed in the WARP model. We used a nanohole cathode with parameters similar to Ref. [1] and conducted a full time-dependent simulation where a laser pulse of variable duration propagates toward the cathode (see Fig. 4, left column). A spectral analysis of the reflected pulse shown in Fig. 4 (right column) provides information on the resonant absorption frequency. In this simulation, the sides of the computational domain are taken to have periodic boundary conditions while the injection and cathode sides have open and perfect conductor boundaries, respectively.

In this simulation, the initial laser pulse is taken to have its spectrum centered at a wavelength of $\lambda = 800$ nm and the nanohole periodicity is chosen to be 769 nm. For sufficiently long laser pulse durations, we observe that the reflected laser spectrum is strongly suppressed for wavelengths around $\lambda \simeq 766$ nm, as expected. Finally, Fig. 4 (right)

depicts the electric field intensity distribution across the nanohole surface. The areas denoted in red correspond to the areas of greatest field enhancement and would produce the strongest particle emission. It is therefore expected that the particle distribution generated by this type of field emitter would have a rich structure with localized regions of enhanced charge that are predominantly originating from the edge of the nanohole and along the direction of the incident electric field polarization.

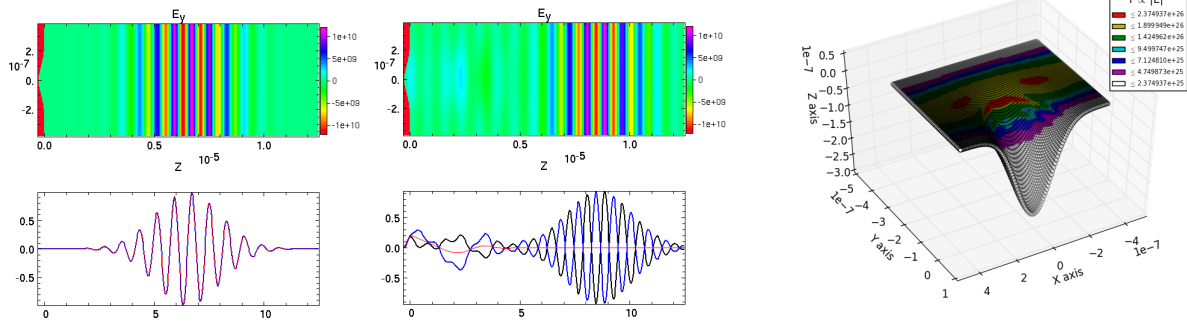


FIGURE 4. LEFT: Snapshots of the incident (left column) and reflected (middle column) laser pulse on the nanohole photocathode located on the left side of the computational domain. For each case, the upper plot depicts the E_y field strength while the lower plot depicts E_y (black), $B_x c$ (blue), and $E_y + B_x c$ (red) as a function of the axial coordinate. RIGHT: Field intensity ($\propto E^2$) distribution on the nanohole cathode surface.

SUMMARY

To conclude, we have developed a simulation to model optically-enhanced field emission from structured cathodes within the WARP framework. The preliminary results suggest our simulation reasonably agrees with previous results. These simulations will be used to provide detailed input for start-to-end simulations of new compact accelerator-based coherent light sources such as the one presented Ref. [2].

ACKNOWLEDGMENTS

This work was supported by DOE contract No. DE-AC02-07CH11359 with the Fermi Research Alliance, LLC, and No. DE-FG02-08ER41532 with Northern Illinois University. The development of WARP is funded by DOE contract No. DE-AC02-05CH11231 with Lawrence Berkeley National Laboratory.

REFERENCES

1. R. K. Li, et al., Phys. Rev. Lett. **110**, 074801 (2013).
2. W. S. Graves, et al., Phys. Rev. Lett. **108**, 263904 (2012).
3. R. H. Fowler and L. Nordheim, Proc. R. Soc. Lond. A **119**, 173 (1928).
4. P. Piot, et al. unpublished (2014).
5. K. L. Jensen, et al. Sol. State Electr. **45**, 831 (2001).
6. P. Hommelhoff, et al., Phys. Rev. Lett. **96**, 077401 (1996).
7. The WARP framework is available via GITHUB at <https://bitbucket.org/berkeleylab/warp>.
8. J. L. Vay, D. P. Grote, R. H. Cohen, and A. Friedman, Comput. Sci. Disc. **5** 014019 (2012).
9. P. Piot, et al. Appl. Phys. Lett. **104**, 263504 (2014).
10. A. Wisitsora-at, et al., J. Vac. Sci. Tech. B: **21**, 1671 (2003).
11. B. E. Carlsten, Nucl. Instrum. Meth. A **285**, 313 (1989).
12. X. Qiu, K. Batchelor, I. Ben-Zvi, X.J. Wang, Phys. Rev. Lett. **76**, 3723 (1996).
13. C. A. Brau, (Vanderbilt University) private communication (2013).
14. D. Mihalcea, unpublished (2014).